Seasonal Modulations of Different Impacts of Two Types of ENSO Events on Tropical Cyclone Activity in the Western North Pacific

Chunzai Wang [1]

Chunxiang Li [2 & 3]

Mu Mu [4]

Wansuo Duan [3]

[1] NOAA Atlantic Oceanographic and Meteorological Laboratory
Miami, Florida

[2] Graduate University of Chinese Academy of Sciences
Beijing, China

[3] LASG/Institute of Atmospheric Physics
Chinese Academy of Sciences
Beijing, China

[4] Key Laboratory of Ocean Circulation and Wave/Institute of Oceanology
Chinese Academy of Sciences
Qingdao, China

Submitted to *Climate Dynamics*

March 2012

Corresponding author address: Dr. Chunzai Wang, Physical Oceanography Division, NOAA/Atlantic Oceanographic and Meteorological Laboratory, 4301 Rickenbacker Causeway, Miami, FL 33149. E-mail: Chunzai.Wang@noaa.gov.

Abstract

The paper examines different impacts of eastern Pacific warm/cold (EPW/EPC) and central Pacific warm/cold (CPW/CPC) events on tropical cyclones (TCs) in the western North Pacific (WNP) by considering the early season of April-June (AMJ), the peak season of July-September (JAS) and the late season of October-December (OND). During AMJ, EPW (EPC) is associated with a significant increase of the TC genesis number in the southeastern (southwestern) sub-region of the WNP, but no class of ENSO events shows a significant change in the TC lifetime and intensity. During JAS, EPW corresponds to an increase (decrease) of the TC genesis number in the southeastern (northwestern) sub-region, but CPW shows no significant change. EPC increases the TC genesis in the northwestern and northeastern sub-regions and decreases the genesis in the southwestern sub-region, whereas CPC suppresses the genesis in the southeastern sub-region. Both the lifetime and intensity of TCs are increased in EPW, but only a shortened lifetime is seen for CPC. During OND, EPW reduces the TC genesis in the southwestern and northwestern sub-regions, whereas CPW enhances the genesis in the southeastern sub-region. Over the South China Sea, CPW and CPC show a significant decrease and increase of the TC genesis, respectively. The TC lifetime is significantly longer in both EPW and CPW and shorter in EPC, and TCs tend to be more (less) intense in EPW (CPC). All of these variations are consistent with the development of ENSO-related SST anomalies during different seasons and are supported by distributions of the genesis potential index – a combination of large-scale oceanic and atmospheric factors that affect TC activity.

TCs in the WNP mainly take the straight westward, northwestward and recurving tracks. During AMJ of EPW years, the TC steering flow patterns favor the recurving track and suppress the straight westward and northwestward tracks. During JAS, EPW is associated with the steering flows that are unfavorable for TCs to move northwestward or westward, whereas CPW favors the northwestward track and suppresses the straight westward track. The steering flow patterns during OND are similar to those during JAS, except that EPC may increase the possibility of the northwestward track.

1. Introduction

El Niño-Southern Oscillation (ENSO) is one of the most important climate phenomena affecting tropical cyclone (TC) activity. About 27 TCs are formed in the western North Pacific (WNP) each year, which accounts for approximately one-third of global TCs. Many studies have examined the relationship between ENSO and TC activity in the WNP (e.g., Chan 2000; Wang and Chan 2002; Camargo and Sobel 2005; Zhao et al. 2010). There is a general consensus that during El Niño events, TC activity significantly increases in the southeastern quadrant of the WNP due to the eastward expansion of the western Pacific warm pool, and decreases in the northwestern quadrant. Due to the eastward shift of the TC genesis region during El Niño, the fetch over which TCs travel and develop expands zonally, allowing TCs to become more intense and have a longer lifetime. Meanwhile, since TCs are formed farther east during El Niño, they are also more likely to recurve northward to higher latitudes while still over water. The opposite tends to be true during La Niña events. There is also a notable TC frequency reduction in the summer following an El Niño year, corresponding to an opposite (westward) longitudinal shift of the zonal SST gradient and Walker circulation and the influence of the tropical Indian Ocean (e.g., Du et al. 2011).

Recently, ENSO events have been separated into two types due to the different spatial distribution of the maximum SST anomalies (Larkin and Harrison 2005; Ashok et al. 2007; Yu and Kao 2007; Kao and Yu 2009; Yu and Kim 2010). For eastern Pacific ENSO events (also called canonical or conventional ENSO events), the maximum SST anomalies are generally located in the cold tongue region of the eastern Pacific. In contrast, central Pacific

ENSO events (also called ENSO Modoki or Dateline ENSO) are characterized by the maximum SST anomalies in the central Pacific further west than the canonical ENSO (can be more than 50° westward). The two types of ENSO events appear to induce distinct climatic and synoptic variability in various regions around the globe (e.g., Weng et al. 2007; Ashok et al. 2009; Cai and Cowan 2009; Wang and Wang 2012). Wang et al. (2012) provide an ENSO overview including the two types of ENSO events and their different climate impacts and mechanisms.

Chen and Tam (2010) and Chen (2011) argued that the distinct heating distribution of El Niño Modoki and canonical El Niño events could induce different atmospheric circulations in the WNP and thus result in distinct impacts on the TC frequency. The warming of canonical El Niño (El Niño Modoki) is associated with an anomalous low-level anticyclone (cyclone) in the WNP, thus resulting in a suppressed (enhanced) convection activity. Kim et al. (2011) compared TC activity in the WNP for three events of the eastern Pacific warming and cooling and the central Pacific warming. They concluded that the east-west extension of the monsoon trough and the change of vertical wind shear play important roles for different TC activity associated with ENSO events having contrasting SST distributions. Hong et al. (2011) further compared the TC landfalls in Taiwan and South China during September to November of canonical El Niño with those of central Pacific El Niño.

Given these previous studies, the present paper mainly focuses on the following topics. First, the paper examines the seasonal modulation of different impacts of the two types of ENSO events on TC activity in the WNP by considering the early season of April to June, the

peak season of July to September, and the late season of October to December. The motivation for examining the seasonal variation is that both ENSO events and TC activity depend upon the season. Second, the paper investigates the relationships of the TC steering flow with the TC tracks for the two types of ENSO events. Third, the paper also extends the study of Kim et al. (2011) by examining the influence of the central Pacific cold event on TC activity in the WNP. Although the cold events in the central and eastern Pacific do not dichotomize to the same extent as warm events (Kug and Ham 2011), it has been shown that the central Pacific cold events also induce remote climate anomalies and ocean circulation change (Cai and Cowan 2009; Shinoda et al. 2011). As shown in this paper, the central Pacific cold event does have different impacts on TC activity in the WNP. Fourth, the paper compares the duration and intensity of TCs contrasting types of ENSO events.

The paper is organized as follows. Section 2 introduces the data sets used in this paper and identifies the years of the two types of ENSO events. Section 3 shows the TC genesis, duration and intensity associated with the two types of ENSO events. Section 4 presents the large-scale environmental factors that affect TC activity in the WNP. Section 5 investigates the relationships of the TC steering flow with the TC tracks during various ENSO events. Finally, section 6 provides a summary and discussion.

2. Data sets and identification of two types of ENSO events

a. Data sets

SST data are taken from the monthly mean Hadley Centre Global Sea Ice and Sea

Surface Temperature (HadISST) data set on a 1° latitude by 1° longitude grid (Rayner et al. 2003). The monthly mean atmospheric data used in this study are the reanalysis data set from the National Centers for Environment Prediction (NCEP)/National Center for Atmospheric Research (NCAR) with a spatial resolution of 2.5°×2.5° (Kalnay et al. 1996). Two TC data sets over the WNP are obtained from Joint Typhoon Warming Center (JTWC) and China Meteorological Administration (CMA), which span the period of 1950 to 2009. A TC is defined as having a maximum surface wind greater than 17 m/s. Since both TC data sets were independently compiled for the same TCs in the WNP, they show some discrepancies as demonstrated in other studies (e.g., Song et al. 2010; Ren et al. 2011). We use both TC data sets in our analyses, but we mainly present the results from the CMA data set since most of the results emphasized in this paper are also basically true for using the JTWC data set. Here we mainly discuss the common and statistically significant results from both TC data sets.

b. Identification of two types of ENSO events

Because the locations of maximum SST anomalies are different, El Niño events have been separated into two types: Eastern Pacific (EP) and Central Pacific (CP) warming events. Several methods have been proposed to identify the two types of ENSO events, ranging from the combination or transformation of Niño indices to the empirical orthogonal function analyses (e.g., Trenberth and Stepaniak 2001; Ashok et al. 2007; Kao and Yu 2009; Kug et al. 2009; Ren and Jin 2011; Takahashi et al. 2011). Wang et al. (2012) provide an overview of

ENSO and the methods for identifying the two types of ENSO. In this paper, we use a simple method to classify EP and CP warm/cool events based on the Nino3 (5°N-5°S, 150°W-90°W) and Nino4 (5°N-5°S, 160°E-150°W) SST anomalies as well as SST spatial distribution. EPW (EPC) events are defined if the 5-month running means of SST anomalies in the Nino3 region exceed 0.5°C (-0.5°C) for more than 6 months and the maximum SST anomalies are located in the eastern Pacific (i.e., the Nino3 SST anomalies are larger than the Nino4 SST anomalies). CPW (CPC) events are associated with the maximum SST anomalies in the central Pacific and requires that the 5-month running means of SST anomalies in the Nino4 region exceed 0.5°C (-0.5°C) for at least 6 months. Based on these criteria and the SST data from 1950 to 2009, 8 EPW years (1951, 1957, 1965, 1972, 1976, 1982, 1987, 1997), 8 EPC years (1955, 1964, 1967, 1971, 1984, 1985, 1988, 2007), 5 CPW years (1969, 1991, 1994, 2002, 2004) and 5 CPC years (1973, 1975, 1989, 2000, 2008) are thus identified. The composites of SST anomalies for EPW, EPC, CPW and CPC events during the mature phase of ENSO are shown in Fig. 1, which are consistent with other studies.

3. TC activity associated with two types of ENSO events

a. Location of TC formation

As stated in the Introduction, previous studies have shown that ENSO's impact on TC activity in the WNP is region-dependent. As in other studies (e.g., Wang and Chan 2002; Zhao et al. 2011; Kim et al. 2011), the tropical WNP of 0°-35°N, 120°E-180°E is partitioned

into four sub-regions: 140°E and 17°N serve as the borders between the east and west and between the south and north, respectively. Additionally, we also consider TC activity in the South China Sea. The five sub-regions of the South China Sea, the southwestern, northwestern, northeastern and southeastern portions of the tropical WNP are represented by SCS, SW, NW, NE and SE, respectively (Fig. 2). The numbers of the climatological TC genesis in SCS, SW, NW, NE and SE are 4.8, 6.1, 5.0, 4.3 and 6.4 per year, respectively. The TC genesis number in the SCS is the smallest among the five sub-regions.

To examine the seasonal modulations of the two types of ENSO events on TC activity, we divide April to December into the early season of April to June (AMJ), the peak season of July to September (JAS) and the late season of October to December (OND). The climatological TC genesis number from the early to late seasons is shown in Table 1. The active genesis location is in the SW sub-region during the early season of AMJ, then shifts northward to the NW sub-region during the peak season of JAS, and finally falls back to the SE sub-region during the late season of OND. If we consider all seasons together, the genesis number of TCs is the largest in the SE sub-region during April to December.

We composite the TC number anomalies with the two types of ENSO events during the different seasons and over the different sub-regions (note that the entire WNP includes the SCS), as shown in Fig. 3. Dot- (cross-) filled bars indicate statistically significant above (below) climatology at the 90% confidence level. During the early season of AMJ, the TC number in EPW (EPC) is significantly increased over the SE (SW) sub-region of the WNP. However, there is no statistically distinct difference of the frequency between CP ENSO

events and climatology in all sub-regions during AMJ. During the peak season of JAS, the TC genesis number shows a SE-NW seesaw pattern in EPW years: TCs increase (decrease) in the SE (NW) sub-region. The TC genesis number during EPC years is enhanced in the NW and NE sub-regions, whereas it is suppressed in the SW sub-region. There is no pronounced change in any sub-region during the peak season of CPW years, but TCs decrease notably in the SE sub-region during CPC years. For the late season of OND, the TC genesis number during CPW years is enhanced in the SE sub-region, but reduced in the SW and NW sub-regions during EPW years. The late season is the only season during which the TC genesis number in the SCS shows a significant change associated with the ENSO event types. CPW (CPC) years correspond to a decreased (increased) TC formation in the SCS.

If we consider all seasons of April to December together (Fig. 3d), the TC number of EPW years increases in the SE sub-region and decreases in the NW and NE sub-regions. There is a distinct increase of TCs in the NE and NW sub-regions during EPC years. The most remarkable changes occur in the SE sub-region for CP ENSO events: TCs obviously increase for CPW events, while they decrease for CPC events. If we consider all sub-regions together as the entire WNP, the only significant TC change is in the late season of EPW years, which shows a decrease in TCs. The TC number of the entire WNP is not sensitive to the two types of ENSO events. This is because TC activity in the WNP is region-dependent and the ENSO influences may cancel each other if we consider the WNP as one region.

b. TC duration and intensity

In this sub-section, we examine the impact of the two types of ENSO events on the duration and intensity of TCs in the WNP. The duration and intensity are measured by TC lifetime in days and maximum sustained surface wind (MSW), respectively. A box-and-whisker diagram is used here to display five-number summaries: the smallest value, lower quartile, median, upper quartile, and largest value. Figure 4 shows the box-and-whisker plots of TC duration associated with the two types of ENSO events. During the early season of AMJ, TCs tend to have slightly longer lifetime in warm events than cold events (statistically insignificant difference from its climatology), reflecting the fact that the ENSO SST anomalies during AMJ are relatively small since most ENSO events are initiated in the spring. During the peak season of JAS, there is a significant increase of TC lifetime in EPW years because of the southeastward shift of the TC genesis locations associated with the warm SST anomalies in the eastern and central Pacific. Figure 4b also shows a decrease in TC lifetime during the peak season of CPC years. During the late season of OND, TC lifetime is significantly longer during EPW and CPW years, but shorter during EPC years, probably because ENSO events are nearly in their mature phase during OND. If we consider all seasons together (from April to December), Figure 4d shows that TC lifetime is significantly longer during EPW years and shorter during CPC years.

As shown in Fig. 5, TCs tend to be a bit more intense in both types of warm events (especially in CPW event) during the early season of AMJ. During the peak season of JAS, Figure 5b shows a statistically significant increase of TC intensity during EPW years because

warmer water extends eastward and TCs thus pass through a vaster region of warm water on their westward tracks. During the late season of OND, a significant increase and decrease of TC intensity occur during EPW and CPC years, respectively. If considering all three seasons together (from April to December), there is a statistically significant tendency toward more (less) intense TCs in EPW (CPC) events as compared to climatology, but there is no significant change in EPC and CPW events.

In summary, the influence of ENSO events on TC lifetime and intensity is not significant in the early season and gradually increases with the development of ENSO events. That is to say, the pronounced change occurs particularly in the peak and late seasons because the ENSO SST anomalies are small during the early season. Overall, there is a tendency for TCs to be longer-lived (shorter-lived) and more (less) intense in warm (cold) events especially in EPW (CPC) events.

4. Large-scale environmental factors

TC activity is influenced by large-scale dynamical and thermodynamical factors (e.g., Gray 1979). Table 2 shows the correlations of various atmospheric variables with the number of TCs in the entire WNP and its five sub-regions. Note that the values underlined represent the correlations being statistically significant in both the CMA and JTWC data sets. Not surprisingly, these variables do not show any significant correlation over the entire WNP during ENSO events since some sub-regions in the WNP are typically favorable for TC activity while others are not, as shown in previous sections (i.e., their effects can cancel each

other if the WNP is considered as a whole). In all sub-regions, at least one environmental variable is significantly correlated with the number of TCs. We would like to point out that in the SE sub-region of the WNP, all variables of the 850-hPa relative vorticiy, 500-hPa pressure vertical velocity, 200-hPa divergence, moist static energy and vertical wind shear (VWS) are significantly correlated with the number of TCs. This is consistent with the results in previous sections that TC activity in the SE sub-region shows a large variation associated with ENSO.

However, the positive correlation with VWS in the SE sub-region is a little bit surprising since it is expected that a reduced (enhanced) VWS is favorable (unfavorable) for the formation and development of TCs as in the case of the North Atlantic. To examine why this happens in the WNP, we plot the maps for VWS regressed onto the number of TCs in the entire WNP and the number of TCs formed in the SE sub-region (Fig. 6). A positive wind shear regression is located just north of the equator in the western Pacific. This is because ENSO is a dominant climate phenomenon in the tropical Pacific, and the atmosphere and ocean vary with ENSO. During the warm phase of ENSO, the Walker circulation is weakened, which manifests itself as a suppressed convection in the western Pacific and an enhanced convection in the eastern/central Pacific. The positive VWS regression in Fig. 6 indicates an increase of VWS in the western Pacific, consistent with the suppressed convection activity in the western Pacific associated with a warm event. However, Figure 6b shows that an east-west band of the negative wind shear is located north of the positive wind shear (also in Fig. 6a). This negative wind shear pattern is favorable for the formation

and development of TCs.

In fact, TC activity in the WNP is influenced by the combination of all large-scale environmental factors. Emanuel and Nolan (2004) proposed an empirical index of the Genesis Potential Index (GPI) for considering the influence of atmospheric and oceanic variables on TC genesis. The GPI combines several large-scale environmental factors including the absolute vorticity, relative humidity, VWS and the potential intensity (PI; Emanuel 1988). The PI is defined as an upper bound of intensity that a TC may reach under a given suite of environmental thermodynamic and dynamical conditions, which depends on the sea level pressure, SST, air temperature and mixing ratio (Bister and Emanuel 2002). The GPI is calculated as follows:

$$GPI = \left|10^5 \eta\right|^{3/2} \left(\frac{H}{50}\right)^3 \left(\frac{PI}{70}\right)^3 (1 + 0.1 V_{shear})^{-2},$$

where η is the absolute vorticity at 850 hPa, H is the relative humidity at 700 hPa and V_{shear} is the VWS magnitude between 200 hPa and 850 hPa. More detailed information about the calculation can be found in Emanuel and Nolan (2004) and Camargo et al. (2007).

Figures 7-9 show the climatological GPI and composites of GPI anomalies in EPW, EPC, CPW and CPC during three seasons of AMJ, JAS and OND, respectively. Climatologically, the maximum values of the GPI display a SE-NW orientation, consistent with the distribution of TC genesis. Large GPI is farther southward during the early and late seasons of AMJ and OND than that during the peak season of JAS. This indicates that atmospheric and oceanic

conditions during the early and late seasons are favorable for TCs to form in the south and that TCs tend to take a track straight westward, whereas during the peak season they are favorable for TCs to form in the north and along a northwestward track.

For EPW events, the SE sub-region of the WNP shows the positive GPI anomalies during all three seasons, whereas other sub-regions display the negative GPI anomalies. The positive GPI anomalies shift eastward as the season progresses from the early season to the late season, reflecting the development of EPW events with the maximum warm SST anomalies in the eastern Pacific toward the winter. For EPC events, the GPI anomaly distributions are approximately a mirror image of EPW events.

For CPW events, the positive GPI anomalies in the SE sub-region shift westward in comparison with those for EPW events, consistent with that the maximum SST anomalies for CPW and EPW events are located in the central and eastern Pacific, respectively. Interestingly, a band of positive GPI anomalies crosses the entire WNP from the SE sub-region to the southeast coast of China, especially during the peak and early seasons of CPW years. This suggests that during CPW years atmospheric and oceanic conditions are favorable for TCs to take the northwestward track – TCs are more likely to make landfall in eastern China during CPW years. For CPC events, all three seasons show the negative GPI anomalies in the SE sub-region. However, the positive GPI anomalies appear in the east of the Philippines and the SCS during the early and late seasons, whereas the positive anomalies are in the NW sub-region during the peak season. This suggests that during the early and late seasons of CPC years, atmospheric and oceanic conditions are favorable for TCs to form

in the south and TCs tend to take the straight westward track, but during the peak season of CPC years TCs are easily formed in the NW sub-region and take the northwestward and recurving tracks. The positive GPI anomalies in the SCS during the late season of CPC years (Fig. 9d) is consistent with Fig. 3c, showing a significant increase of TCs formed in the SCS during OND of CPC years.

5. TC tracks and steering flow

TC track density in the WNP is calculated by counting the number of TCs forming within and passing through each 5°×5° grid box for a given season. The climatology of TC track density displays a maximum over the sea northeast of the Philippines (not shown), reflecting that most TCs form in the tropical WNP and move westward and northwestward. Previous studies have classified three prevailing TC tracks: (1) the westward track across the Philippines and the SCS to the southeast of China and Vietnam, (2) the northwestward track toward the east coast of China, and (3) the recurving track toward the regions near Japan and the sea east of Japan (e.g., Liu and Chan 2008). As the TC movement is primarily controlled by the surrounding environmental flow and modified by the beta-effect, here we examine the TC steering flow which is calculated as the vertically-averaged wind from 850 hPa to 300 hPa. We calculate the composites of TC track density and steering flow anomalies for the two types of ENSO events during different seasons.

During the early season of AMJ, an anomalous cyclonic steering flow is located over eastern China in EPW events (Fig. 10a). Associated with the cyclone are the anomalous

northeastward steering flows in the subtropical western Pacific and the anomalous westerly steering anomalies in the tropical western Pacific. This steering flow pattern favors the recurving track and suppresses the westward and northwestward track. As a result, the TC track density is increased in the open ocean of the WNP and decreased in the SCS and the southeast coast of China (Fig. 10a). For EPC events, the anomalous easterly steering flows occupy the subtropical region north of 20°N, which is associated with an increase of TC track density in the northern SCS and the south of China and a decrease of TC track density over the eastern sea board of China and Japan (Fig. 10b). For CPW events, the great changes of TC track density mainly occur in the tropical region near 18°N and 136°E (Fig. 10c). For CPC events, an anomalous cyclone of the TC steering flow is centered over Japan, which corresponds to the negative anomalies of TC track density in nearly the entire WNP.

During the peak season of JAS, associated with the negative and positive anomalies of TC track density in the NW and SE sub-regions for EPW events are the westerly and easterly steering flow anomalies, respectively (Fig. 11a). This indicates that during the peak season of EPW years TCs are less likely to move northwestward or westward, consequently making landfall in the southeast coast of China. For EPC events, the positive anomalies of TC track density are concentrated in the north of the WNP, due to the increase of TCs formed there in EPC years. For CPW events, an anomalous anticyclonic steering flow occupies the sea east of Japan, and the westerly steering flow anomalies prevail in the tropics. Associated with these TC steering patterns, more TCs move northwestward but less move westward. In other words, during JAS of CPW years the probability of the northwestward track is

increased, but the possibility of the straight westward track is decreased. For CPC events, the negative anomalies of TC track density are in the eastern part of the WNP due to the CPC-induced decrease of TC genesis. The positive anomalies of TC track density in the east coast of China are due to the increased number of TCs formed in the NW sub-region during CPC years.

The distributions of the track density and steering flow anomalies during the late season of OND are approximately similar to those during the peak season of JAS. However, two differences are worthy of note. First, during OND of EPC years the strong northward and northwestward steering flow anomalies are located east of the Philippine Sea and in the sea of eastern China, which may favor for the northwestward track. Second, the TC steering flow patterns during OND of CPW years are much stronger than those during JAS. Thus, the strong northwestward steering flow anomalies appear in the NW sub-region of the WNP, and the strong westerly steering flow anomalies are located in the SCS, the south of China and Vietnam. This suggests that during OND of CPW years TCs are more likely to move northwestward to Japan and/or recurve eastward, and few TCs can make landfall in Vietnam and the south coast of China.

6. Summary and discussion

Since the influences of ENSO on TC activity in the WNP are region-dependent, we separate the WNP into the five sub-regions of the SCS, SW, NW, NE and SE (Fig. 2). We also examine the seasonal variations of TC activity by considering the early season of AMJ,

1 the peak season of JAS and the late season OND. Climatologically, the active TC genesis
2 location is in the SW sub-region during the early season of AMJ, then shifts northward to the
3 NW sub-region during the peak season of JAS, and finally falls back to the SE sub-region
4 during the late season of OND. If we consider all seasons together from April to December,
5 the largest and smallest TC genesis numbers are in the SE and SCS sub-regions, respectively.
6 The combination of large-scale environmental factors of the genesis potential index (GPI)
7 indicates that atmospheric and oceanic conditions during the early and late seasons are
8 favorable for TCs to form in the south and TCs tend to take the straight westward track,
9 whereas during the peak season they are favorable for TCs to form in the north and the
10 northwestward track.

11 The early season of AMJ, EPW (EPC) is associated with a significant increase of the TC
12 genesis number in the SE (SW) sub-region of the WNP, but both CPW and CPC show no
13 statistically distinct difference of the TC genesis from climatology in all sub-regions. All
14 ENSO events show no significant change in TC lifetime and intensity. The increase in TC
15 genesis in the SE sub-region during AMJ of EPW years is consistent with and supported by
16 the SE positive anomalies of the GPI – a combination of large-scale atmospheric and oceanic
17 factors that affect TC activity. The insignificant change of TC lifetime and intensity reflects
18 that most ENSO events are initiated during the spring and the ENSO-related SST anomalies
19 are too small to affect TC lifetime and intensity during AMJ.

20 During the peak season of JAS, EPW corresponds to an increase (decrease) of the TC
21 genesis number in the SE (NW) sub-region, but CPW shows no significant genesis change in

any sub-regions. EPC increases the TC genesis number in the NW and NE sub-regions and decreases the genesis in the SW sub-region, while CPC suppresses the genesis in the SE sub-region. All of these are consistent with the GPI anomaly distribution, except in the NW and SW sub-regions where the GPI anomalies do not show significant changes during JAS of EPC years. Both TC lifetime and intensity are increased for EPW events, but only TC lifetime is shortened for CPC events. This is consistent with the eastward shift of warm SST anomalies for EPW events while the cold SST anomalies are located farther westward for CPC events.

During the late season of OND, EPW reduces the TC genesis number in the SW and NW sub-regions, whereas CPW enhances the genesis in the SE sub-region. Again, these are consistent with the GPI decreases in the western part of the WNP during OND of EPW years and the GPI increases in the SE sub-region during CPW years. TC lifetime is significantly longer for both EPW and CPW and shorter in EPC, and TCs tend to be more (less) intense for EPW (CPC). This is because the late season of OND is the closest to the mature phase of ENSO events and the ENSO-related SST anomalies are relatively large during that season.

The SCS is the largest semi-enclosed marginal sea in the tropical WNP and most TCs formed there will affect the surrounding land. ENSO influence on TCs formed in the SCS is significant only during the late season of OND because ENSO has a delayed effect on the SCS SST anomalies (Wang et al. 2006). During the late season of OND, CPW is associated with a decrease of TC genesis, whereas CPC corresponds to an increase of TC genesis. Interestingly, it is not found that EPW and EPC have a significant influence on TC genesis in

the SCS. This may be consistent with the recent finding that the eastern Pacific warm events induce an anomalous anticyclone in the WNP, but the central Pacific warm events are associated with an anomalous cyclone near the Philippines (Chen 2011; Wang and Wang 2012). In fact, our calculations do show that the negative GPI anomalies are located in the central SCS during OND of CPW years and the positive GPI anomalies are in the entire SCS during CPC years (Fig. 9).

Many large-scale oceanic and atmospheric factors affect TC activity in the WNP. Because their influences on TCs are determined by the net result of these large-scale environmental factors, this paper focuses on the combination of large-scale factors – the GPI as proposed by Emanuel and Nolan (2004). As discussed in this paper, the GPI anomaly distributions are basically consistent with TC genesis for various ENSO events. We also calculate the individual effect of large-scale environmental factors on TC activity in the WNP. For example, Figure 13 shows the VWS difference between ENSO events and climatology during the peak season of JAS. For both EPW and CPW, the positive VWS anomalies are located north of the equator in the WNP, with the positive anomalies shifting westward in the case of CPW. As stated in Section 4, the positive VWS anomalies reflect the fact that a warm ENSO event suppresses convection activity in the equatorial western Pacific and enhances the convection in the central/eastern Pacific (associated with the weakened Walker circulation). North of the positive VWS anomalies are the negative VWS anomalies which favor for the formation and development of TCs. The VWS distributions for the cold events are similar to the counterparts of the warm events, but with the anomaly sign reversed.

The TC tracks mainly depend on the large-scale atmospheric circulation of the steering flow although they also relate to the TC internal dynamics and synoptic weather patterns. In this paper, we investigate variability of the TC steering flow associated with various ENSO events. During AMJ of EPW years, the northeastward steering flow anomalies in the subtropical WNP and the eastward flow anomalies in the tropical region favor the recurving track and suppress the straight westward and northwestward tracks. During JAS, the steering flow patterns show that EPW is unfavorable for TCs to move northwestward or westward, whereas CPW favors the northwestward track and suppresses the straight westward track. The steering flow patterns during OND are similar to those during JAS, except that EPC is associated with the northward and northwestward steering flow anomalies in the seas of the Philippines and eastern China, which may increase the possibility of the northwestward track.

Previous studies have shown that there is a discrepancy among different TC data sets in the WNP (e.g., Song et al. 2010; Ren et al. 2011). Although this paper attempts to mainly discuss the common features of both the CMA and JTWC TC data sets, the differences among TC data sets associated with various ENSO events deserve further study. In addition, the observed results in this paper need to be tested and confirmed by numerical model experiments. We are currently working on this topic and hope that we can write another manuscript soon.

Acknowledgments. CW thanks Drs. Greg Foltz and David Enfield for serving as internal

reviewers of AOML for this manuscript. This work was supported by grants from National Natural Science Foundation of China (No. 40830955 and 41176013), the Knowledge Innovation Program of Chinese Academy of Sciences (No. KZCX2-YW-QN203), and the National Basic Research Program of China (No. 2010CB950400).

References

Ashok, K., S. K. Behera, S. A. Rao, H. Weng, and T. Yamagata (2007) El Niño Modoki and its possible teleconnection. J Geophys Res 112: C11007, doi:10.1029/2006JC003798.

Ashok, K., and T. Yamagata (2009) Climate change: The El Niño with a difference. Nature 461: 481-484.

Bister, M., and K. A. Emanuel (2002) Low frequency variability of tropical cyclone potential intensity. 1. Interannual to interdecadal variability. J Geophys Res 107: 4801. doi:10.1029/2001JD000776.

Cai, W., and T. Cowan (2009) La Niña Modoki impacts Australia autumn rainfall variability. Geophys Res Lett 36: L12805, doi:10.1029/2009GL037885.

Camargo SJ, Sobel AH (2005) Western North Pacific tropical cyclone intensity and ENSO. J Clim 18: 2996–3006.

Camargo, S. J., K. A. Emanuel, and A. H. Sobel (2007) Use of a genesis potential index to diagnose ENSO effects on tropical cyclone genesis. J Clim 20: 4819-4834.

Chan, J. C. L. (2000) Tropical cyclone activity over the western North Pacific associated with El Niño and La Niña events. J Clim13: 2960–2972.

Chen, G., and C.-Y. Tam (2010) Different impacts of two kinds of Pacific Ocean warming on tropical cyclone frequency over the western North Pacific. Geophys Res Lett 37: L01803, doi:10.1029/2009GL041708.

Chen, G. (2011) How does shifting Pacific Ocean warming modulate on tropical cyclone frequency over the South China Sea? J Clim 24: 4695–4700.

Du, Y., L. Yang, and S.-P. Xie (2011) Tropical Indian Ocean influence on northwest Pacific tropical cyclones in summer following strong El Nino. J Clim 24: 315-322.

Emanuel, K. A. (1988) The maximum intensity of hurricanes. J Atmos Sci 45: 1143-1155.

Emanuel, K. and D. S. Nolan (2004) Tropical cyclone activity and the global climate system. Proc 26 the AMS Conf on Hurr and Trop Meteor 10: 240-241.

Gray, W. M. (1979) Hurricanes: their formation, structure, and likely role in the tropical circulation. In *Meteorology over the tropical oceans,* Ed., D. B. Shaw, Roy Meteor Soc 155-218.

Hong, C.-C., Y.-H. Li, T. Li, and M.-Y. Lee (2011) Impacts of central Pacific and eastern Pacific El Nino on tropical cyclone tracks over the western North Pacific. Geophys Res Lett 38: L16712. doi:10.1029/2011GL048821.

Kalnay, E., and Coauthors (1996) The NCEP/NCAR 40-Year Reanalysis Project. Bull Am Meteorol Soc 77: 437–471.

Kao, H. Y., and J. Y. Yu (2009) Contrasting eastern Pacific and central Pacific types of 468 ENSO. J Clim 22: 615-631.

Kim, H.-M., P. J. Webster, and J. A. Curry (2011) Modulation of North Pacific tropical cyclone activity by three phases of ENSO. J Clim 24: 1839-1849.

Kug, J.-S., and Y.-G. Ham (2011) Are there two types of La Nina? Geophys Res Lett 38: L16704. doi:10.1029/2011GL048237.

Larkin, N. K., and D. E. Harrison (2005) Global seasonal temperature and precipitation anomalies during El Niño autumn and winter. Geophys Res Lett 32: L16705.

doi:10.1029/2005GL022860.

Liu, K. S., and J. C. L. Chan (2008) Interdecadal variability of western North Pacific tropical cyclones tracks. J Clim 21: 4464–4476 .

Rayner, N. A., D. E. Parker, E. B. Horton, C. K. Folland, L. V. Alexander, D. P. Rowell, E. C. Kent, and A. Kaplan (2003) Global analyses of SST, sea ice and night marine air temperature since the late nineteenth century. J Geophys Res 108: 4407. doi:10.1029/2002JD002670.

Ren, F, J Liang, G Wu, W Dong, X Yang (2011) Reliability analysis of climate change of tropical cyclone activity over the western North Pacific. J Clim 24: 5887–5898.

Ren, H.-L., and F.-F. Jin (2011) Niño indices for two types of ENSO. Geophys Res Lett 38: L04704. doi:10.1029/2010GL046031.

Shinoda, T, H. E. Hurlburt, E. J. Metzger (2011) Anomalous tropical ocean circulation associated with La Nina Modoki. J. Geophys. Res. 116, doi:10.1029/2011JC007304.

Song, J.-J., Y. Wang, and L. Wu (2010) Trend discrepancies among three best track data sets of western North Pacific tropical cyclones. J Geophys Res 115: D12128. doi:10.1029/2009JD013058.

Takahashi, K., A. Montecinos, K. Goubanova, and B. Dewitte (2011) ENSO regimes: Reinterpreting the canonical and Modoki El Niño. Geophys Res Lett 38: L10704. doi:10.1029/2011GL047364.

Trenberth, K. E., and D. P. Stepaniak (2001) Indices of El Niño evolution. J Clim 14: 1697-1701.

Wang, B., and J. C. L. Chan (2002) How strong ENSO events affect tropical storm activity over the western North Pacific. J Clim 15: 1643-1658.

Wang, C., W. Wang, D. Wang, and Q. Wang (2006) Interannual variability of the South China Sea associated with El Niño. J Geophy Res 111: C03023. doi:10.1029/2005JC003333.

Wang, C., C. Deser, J.-Y. Yu, P. DiNezio, and A. Clement (2012) El Nino-Southern Oscillation (ENSO): A review. In *Coral Reefs of the Eastern Pacific*, P. Glymn, D. Manzello, and I. Enochs, Eds., Springer Science Publisher.

Wang, C., and X. Wang (2012) El Nino Modoki I and II classifying by different impacts on rainfall in the southern China and typhoon tracks. J Clim, submitted.

Weng, H., K. Ashok, S. K. Behera, A. S. Rao and T. Yamagata (2007) Impacts of recent El Niño Modoki on dry/wet conditions in the Pacific rim during boreal summer. Clim Dyn 29: 113–129.

Yu, J.-Y., and H.-Y. Kao (2007) Decadal changes of ENSO persistence barrier in SST and ocean heat content indices: 1958-2001. *J. Geophys. Res.* 112, D13106, doi:10.1029/2006JD007654.

Yu, J.-Y., and S. T. Kim (2010) Three evolution patterns of Central-Pacific El Niño. *Geophys. Res. Lett.* 37, L08706, doi:10.1029/2010GL042810.

Zhao, H. K., L. G. Wu, and W. C. Zhou (2010) Assessing the infuence of the ENSO on tropical cyclone prevailing tracks in the western North Pacific. Adv Atmos Sc 27: 1361-1371. doi:10.1007/s00376-010-9161-9.

Zhao, H. K., L. G. Wu, and W. C. Zhou (2011) Interannual changes of tropical cyclone intensity in the western North Pacific. J Meteor Soc Japan 89: 243-253.

Figure Captions

Figure 1. Composites of SST anomalies (°C) during the mature phase of ENSO (November to January) for (a) EPW, (b) EPC, (c) CPW, and (d) CPC events.

Figure 2. Spatial distribution of the TC genesis in the WNP during April to December. The WNP is divided into the sub-regions of the SCS, SW, NW, NE and SE. The numbers in the parenthesis represent the climatological numbers of TCs per year formed in these sub-regions.

Figure 3. The TC number anomalies formed in the WNP and its five sub-regions in EPW, EPC, CPW and CPC events. Shown are during (a) the early season of AMJ, (b) the peak season of JAS, (c) the late season of OND, and (d) all seasons from April to December. Dot (cross) filled bars indicate statistically significant above (below) climatology at the 90% confidence level from the CMA data set.

Figure 4. The box-and-whisker plots of TC lifetime (days) associated with EPW, EPC, CPW and CPC events. Shown are during (a) the early season of AMJ, (b) the peak season of JAS, (c) the late season of OND, and (d) all seasons from April to December. ALL represents all years from 1950 to 2009. The box-and-whisker diagram is plotted by using the numbers of the smallest value, lower quartile (Q1), median, upper quartile (Q3), and largest value. The box shows the quartile Q1 and quartile Q3, the line in the box marks the

median, and the dot or asterisk represents the mean. The red (blue) asterisk indicates statistically significant increase (decrease) of mean lifetime at the 90% level.

Figure 5. The box-and-whisker plots of TC intensity (m/s) associated with EPW, EPC, CPW and CPC events. Shown are during (a) the early season of AMJ, (b) the peak season of JAS, (c) the late season of OND, and (d) all seasons from April to December. ALL represents all years from 1950 to 2009. The box-and-whisker diagram is plotted by using the numbers of the smallest value, lower quartile (Q1), median, upper quartile (Q3), and largest value. The box shows the quartile Q1 and quartile Q3, the line in the box marks the median, and the dot or asterisk represents the mean. The red (blue) asterisk indicates statistically significant increase (decrease) of mean intensity at the 90% level.

Figure 6. Regressions (m/s per the number) of vertical wind shear (VWS) onto the number of TCs during July to September (JAS). Shown are for (a) the number of TCs formed in the entire WNP and (b) the number of TCs formed in the SE sub-region of the WNP. The stippling indicates statistically significant at the 90% level. The VWS is calculated as the magnitude of the vector difference between winds at 200 hPa and 850 hPa.

Figure 7. TC genesis potential index (GPI) during the early season of AMJ. Shown are (a) climatological GPI and GPI anomalies in (b) EPW, (c) EPC, (d) CPW, and (e) CPC. White solid (dashed) lines indicate statistically significant increase (decrease) at the 90% level comparing to the climatology.

Figure 8. TC genesis potential index (GPI) during the peak season of JAS. Shown are (a) climatological GPI and GPI anomalies in (b) EPW, (c) EPC, (d) CPW, and (e) CPC. White solid (dashed) lines indicate statistically significant increase (decrease) at the 90% level comparing to the climatology.

Figure 9. TC genesis potential index (GPI) during the late season of OND. Shown are (a) climatological GPI and GPI anomalies in (b) EPW, (c) EPC, (d) CPW, and (e) CPC. White solid (dashed) lines indicate statistically significant increase (decrease) at the 90% level comparing to the climatology.

Figure 10. TC track density (the number) and steering flow anomalies (m/s) during the early season of AMJ. Shown are in (a) EPW, (b) EPC, (c) CPW, and (d) CPC. The steering flow is calculated as the vertically-integrated wind from 850 hPa to 300 hPa, normalized by (850-hPa - 300-hPa). White contours and stippling indicate statistically significant at the 90% level for track density and steering flow, respectively.

Figure 11. TC track density (the number) and steering flow anomalies (m/s) during the peak season of JAS. Shown are in (a) EPW, (b) EPC, (c) CPW, and (d) CPC. The steering flow is calculated as the vertically-integrated wind from 850 hPa to 300 hPa, normalized by (850-hPa - 300-hPa). White contours and stippling indicate statistically significant at the 90% level for track density and steering flow, respectively.

Figure 12. TC track density (the number) and steering flow anomalies (m/s) during the late season of OND. Shown are in (a) EPW, (b) EPC, (c) CPW, and (d) CPC. The steering flow is calculated as the vertically-integrated wind from 850 hPa to 300 hPa, normalized by (850-hPa - 300-hPa). White contours and stippling indicate statistically significant at the 90% level for track density and steering flow, respectively.

Figure 13. Vertical wind shear (VWS) difference (m/s) between ENSO events and climatology during the peak season of JAS. Shown are in (a) EPW, (b) EPC, (c) CPW, and (d) CPC. The stippling indicates statistically significant at the 90% level. The VWS is calculated as the magnitude of the vector difference between winds at 200 hPa and 850 hPa.

Table 1. The climatological numbers of TCs formed in the WNP and its five sub-regions during the early season of AMJ, the peak season of JAS, the late season of OND, and all seasons from April to December.

Region / Season	SCS	SW	NW	SE	NE	WNP
AMJ	0.92	1.40	0.32	0.93	0.10	3.67
JAS	2.58	2.47	4.12	2.58	3.45	15.20
OND	1.30	2.20	0.60	2.90	0.70	7.70
April-December	4.80	6.07	5.03	6.42	4.25	26.57

Table 2. Correlation coefficients of JAS (July to September) 850-hPa relative vorticity (VOR), 500-hPa pressure vertical velocity (VEL), 200-hPa divergence (DIV), moist static energy (MSE) and vertical wind shear (VWS) with the TC formation number in five sub-regions and the entire WNP. The correlations exceeding the 90%, 95%, and 99% confidence levels are represented by *, **, and ***, respectively. The correlations are calculated from the CMA TC data set. The values underlined indicate that they are statistically significant both in the CMA and JTWC TC data sets.

Variable / Region	VOR	VEL	DIV	MSE	VWS
SCS	0.06	-0.30**	0.20	0.14	0.01
SW	0.30**	0.004	0.01	-0.15	0.05
NW	0.26**	-0.23*	0.19	0.15	-0.13
SE	0.46***	-0.51***	0.55***	0.36***	0.57***
NE	0.57***	-0.48***	0.58***	-0.08	-0.24*
WNP	-0.07	-0.07	-0.04	-0.24	0.17

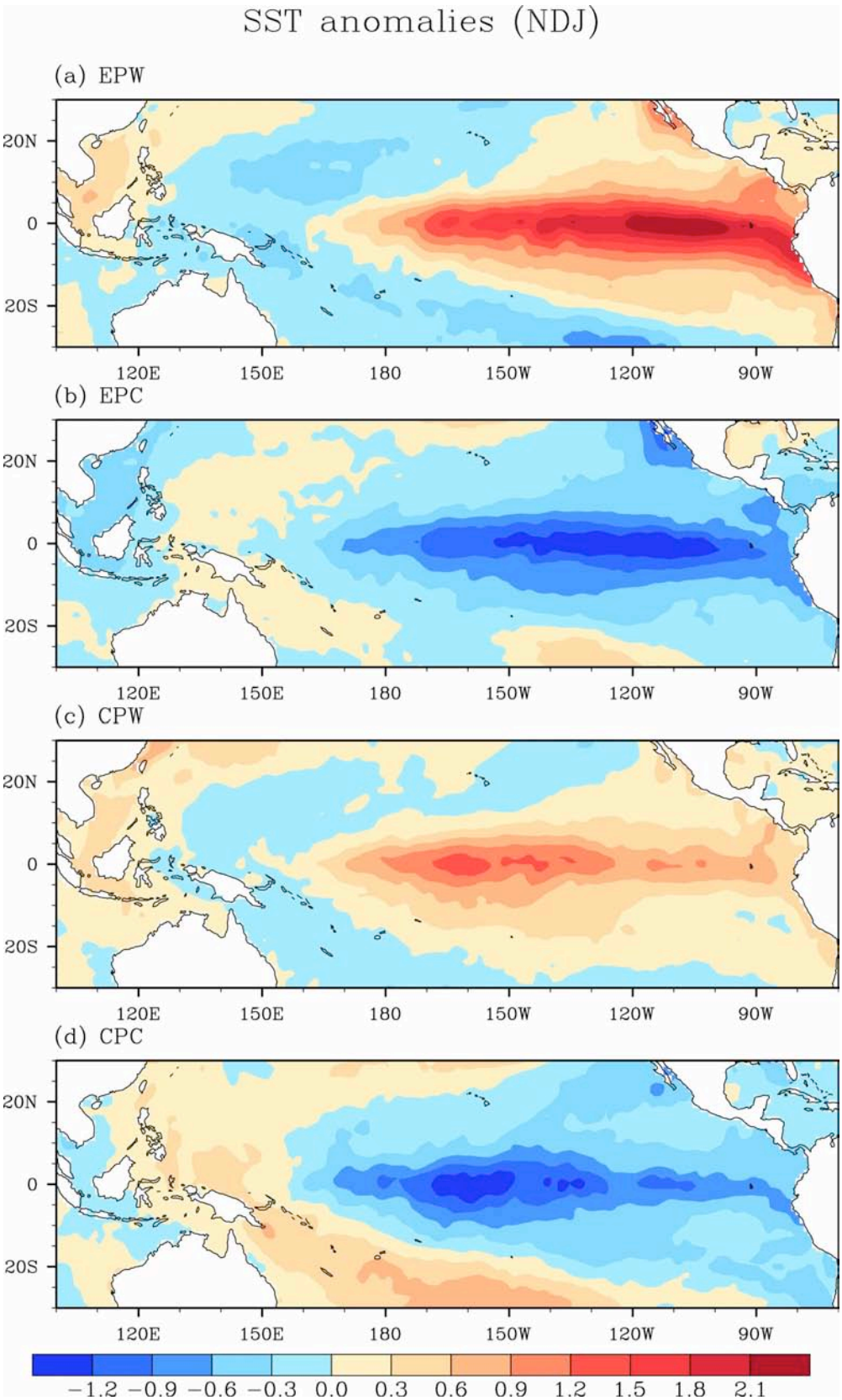

Figure 1. Composites of SST anomalies (°C) during the mature phase of ENSO (November to January) for (a) EPW, (b) EPC, (c) CPW, and (d) CPC events.

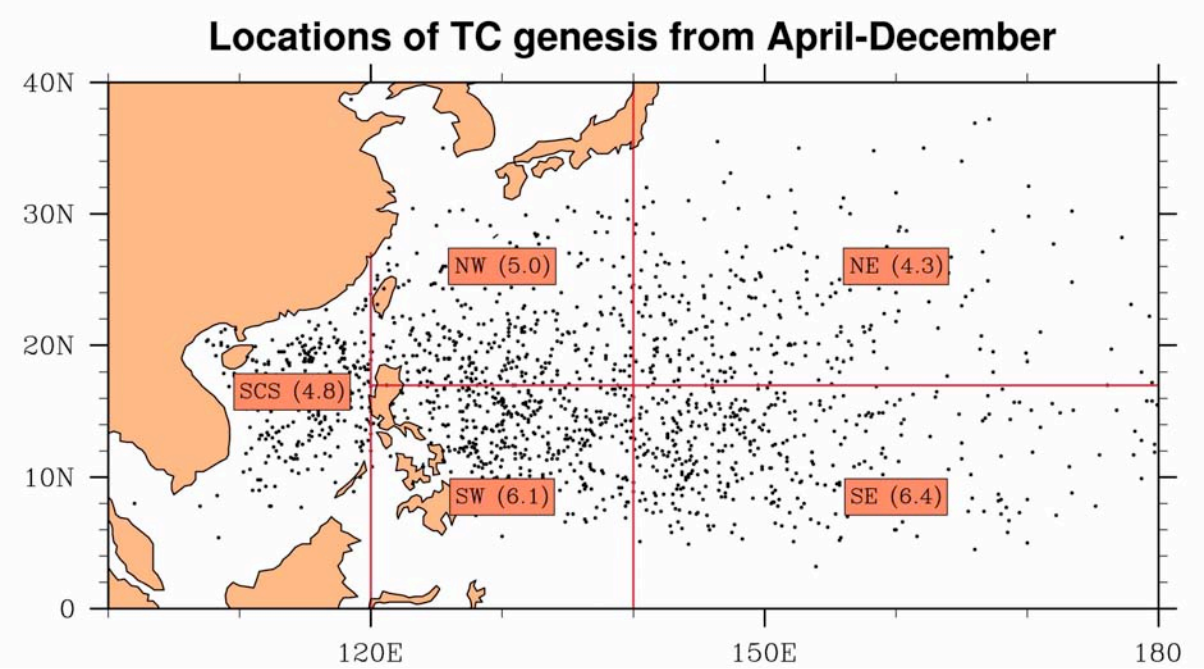

Figure 2. Spatial distribution of the TC genesis in the WNP during April to December. The WNP is divided into the sub-regions of the SCS, SW, NW, NE and SE. The numbers in the parenthesis represent the climatological numbers of TCs per year formed in these sub-regions.

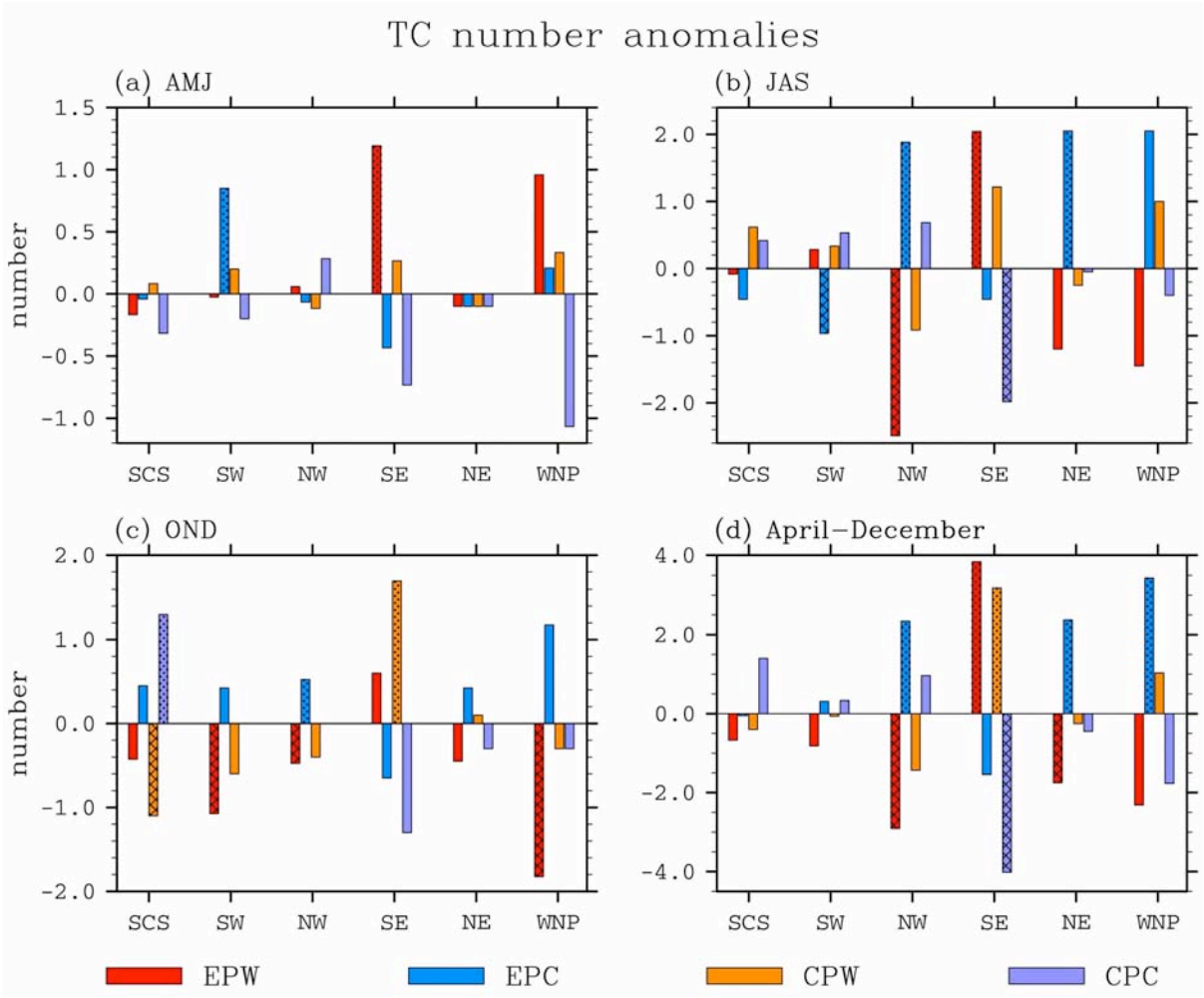

Figure 3. The TC number anomalies formed in the WNP and its five sub-regions in EPW, EPC, CPW and CPC events. Shown are during (a) the early season of AMJ, (b) the peak season of JAS, (c) the late season of OND, and (d) all seasons from April to December. Dot (cross) filled bars indicate statistically significant above (below) climatology at the 90% confidence level from the CMA data set.

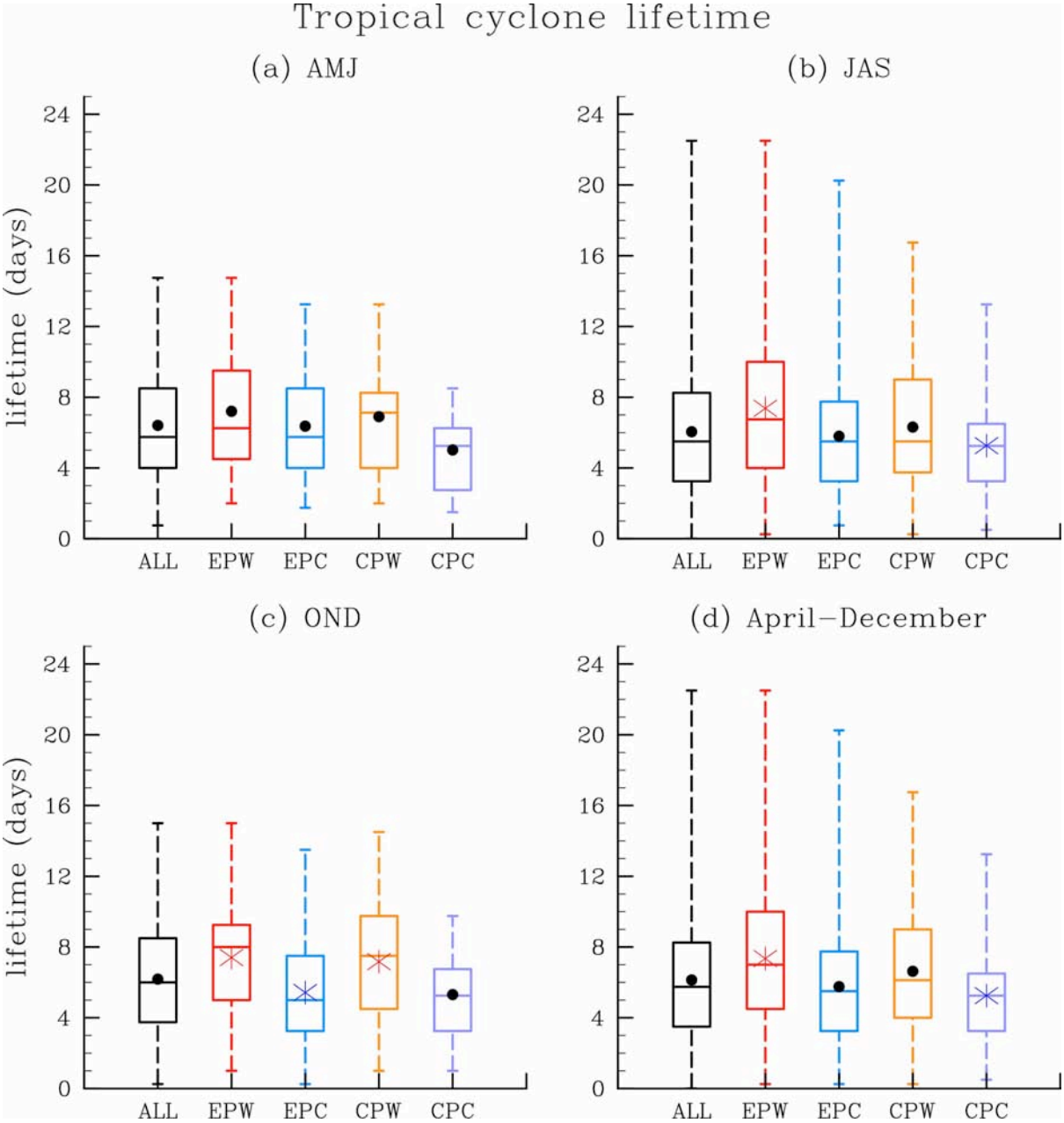

Figure 4. The box-and-whisker plots of TC lifetime (days) associated with EPW, EPC, CPW and CPC events. Shown are during (a) the early season of AMJ, (b) the peak season of JAS, (c) the late season of OND, and (d) all seasons from April to December. ALL represents all years from 1950 to 2009. The box-and-whisker diagram is plotted by using the numbers of the smallest value, lower quartile (Q1), median, upper quartile (Q3), and largest value. The box shows the quartile Q1 and quartile Q3, the line in the box marks the median, and the dot or asterisk represents the mean. The red (blue) asterisk indicates statistically significant increase (decrease) of mean lifetime at the 90% level.

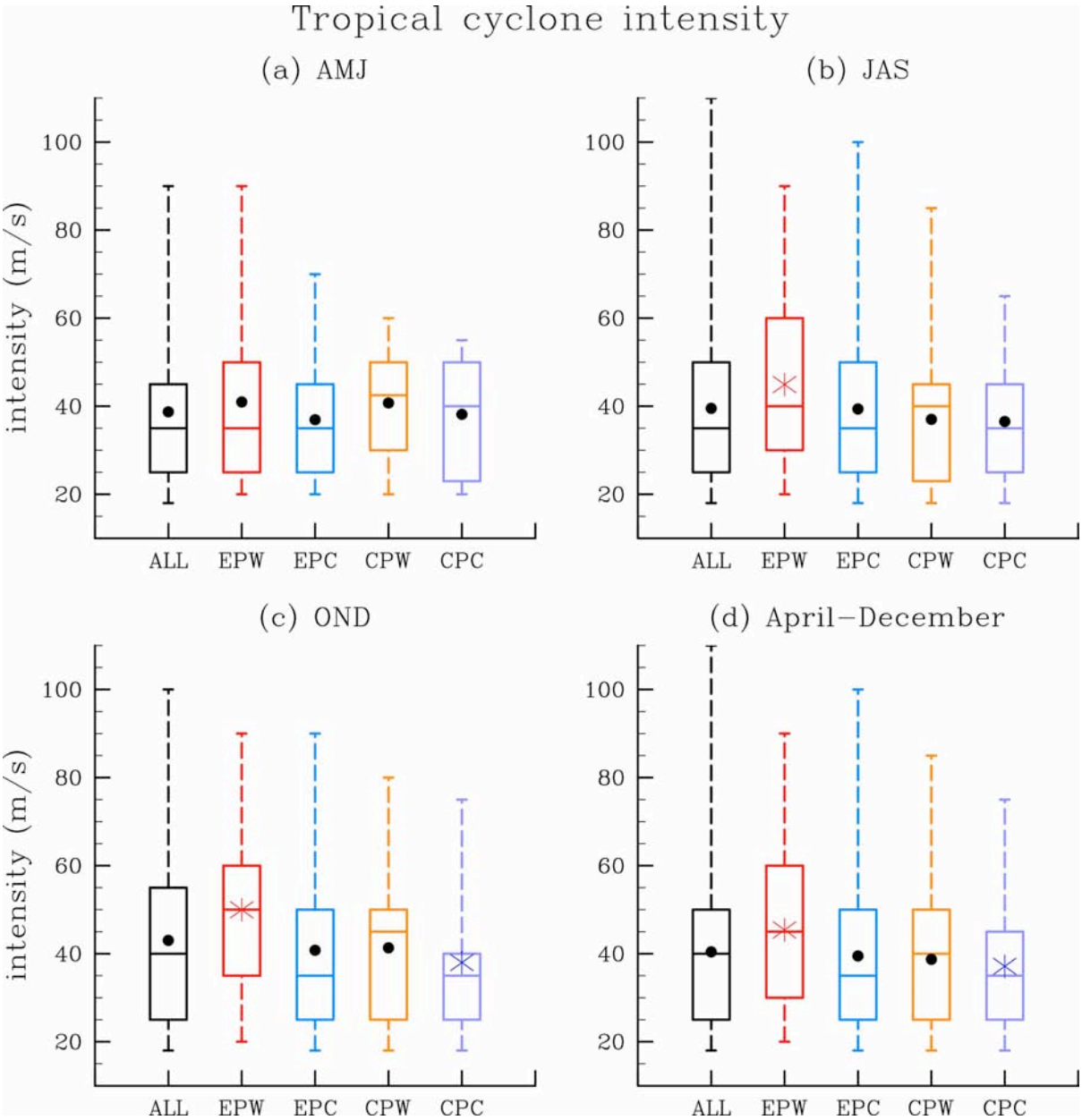

Figure 5. The box-and-whisker plots of TC intensity (m/s) associated with EPW, EPC, CPW and CPC events. Shown are during (a) the early season of AMJ, (b) the peak season of JAS, (c) the late season of OND, and (d) all seasons from April to December. ALL represents all years from 1950 to 2009. The box-and-whisker diagram is plotted by using the numbers of the smallest value, lower quartile (Q1), median, upper quartile (Q3), and largest value. The box shows the quartile Q1 and quartile Q3, the line in the box marks the median, and the dot or asterisk represents the mean. The red (blue) asterisk indicates statistically significant increase (decrease) of mean intensity at the 90% level.

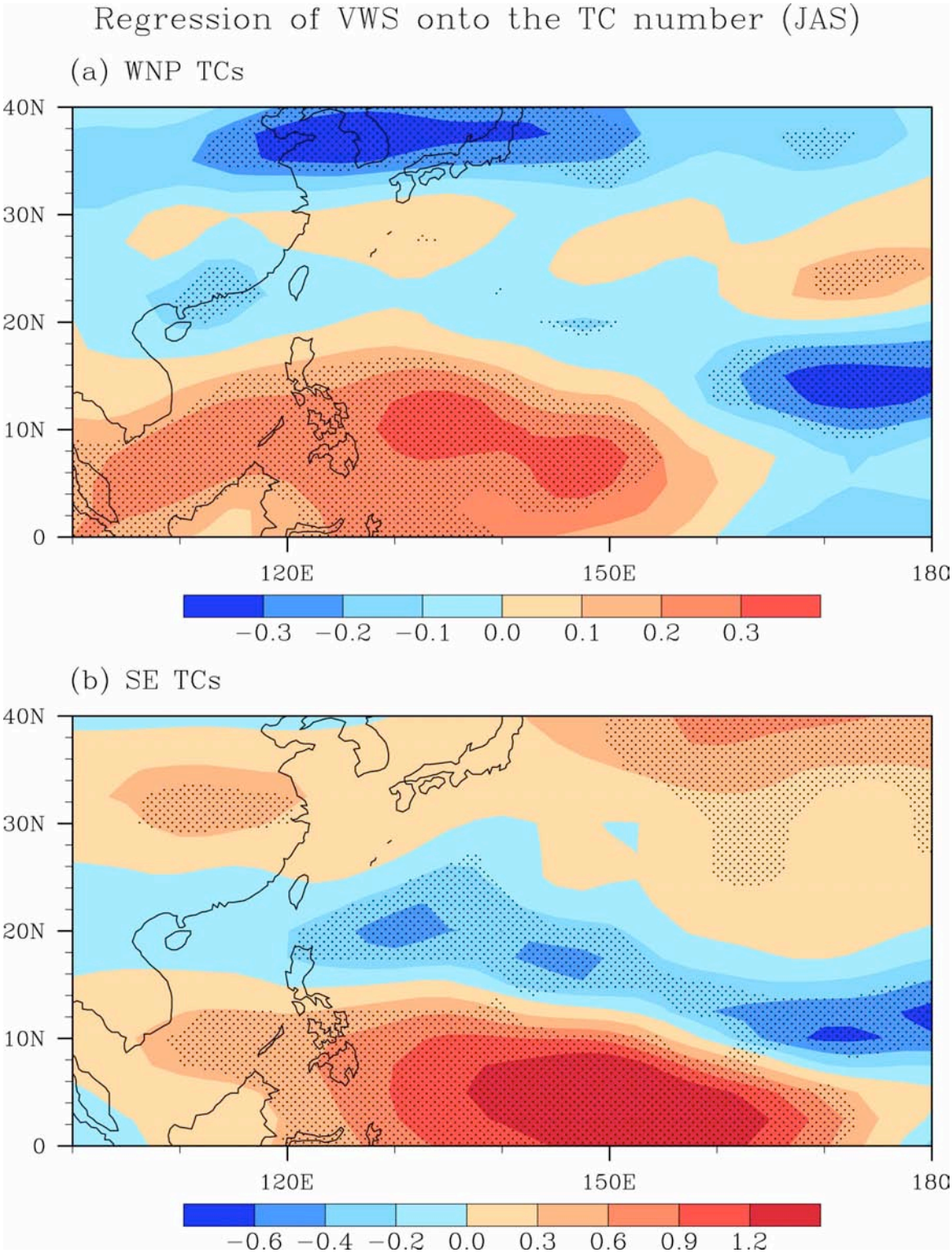

Figure 6. Regressions (m/s per the number) of vertical wind shear (VWS) onto the number of TCs during July to September (JAS). Shown are for (a) the number of TCs formed in the entire WNP and (b) the number of TCs formed in the SE sub-region of the WNP. The stippling indicates statistically significant at the 90% level. The VWS is calculated as the magnitude of the vector difference between winds at 200 hPa and 850 hPa.

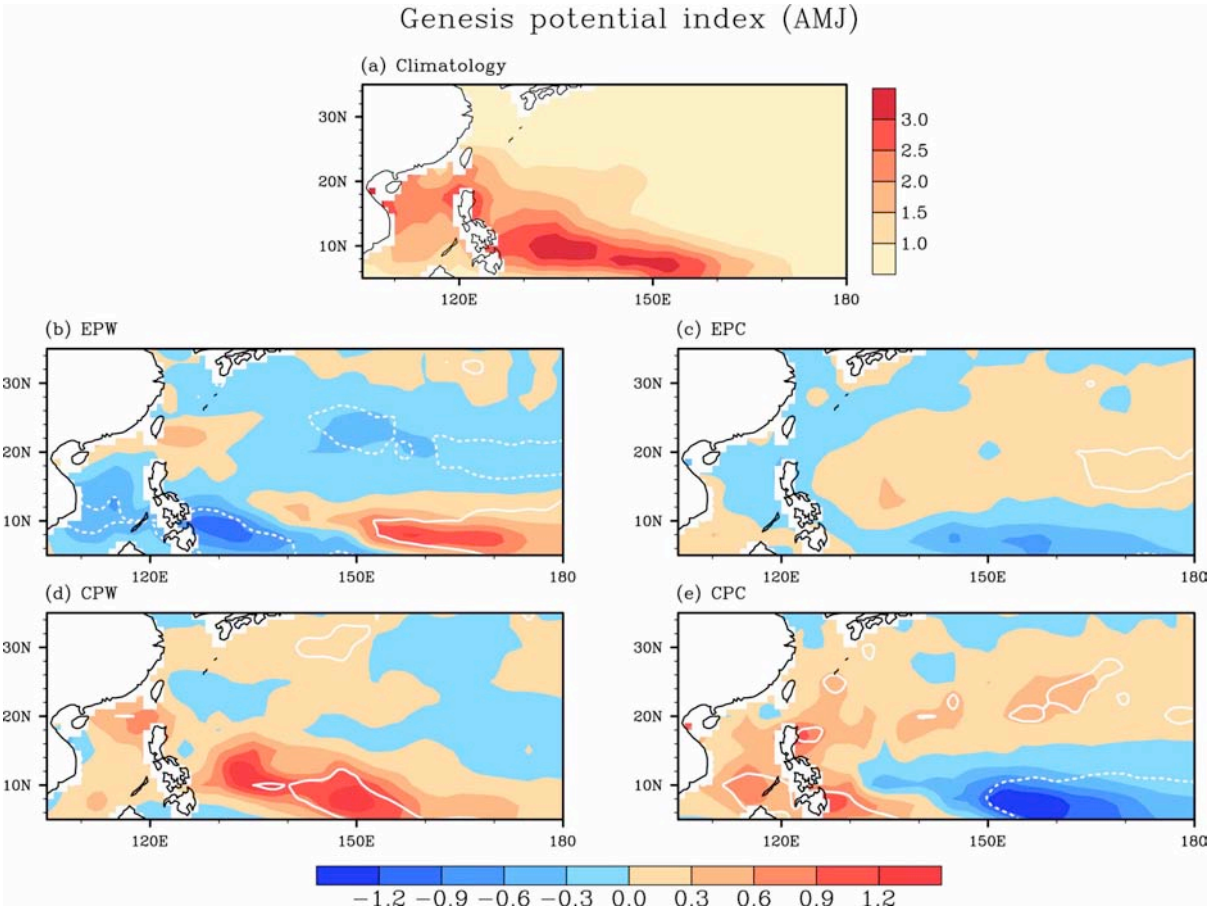

Figure 7. TC genesis potential index (GPI) during the early season of AMJ. Shown are (a) climatological GPI and GPI anomalies in (b) EPW, (c) EPC, (d) CPW, and (e) CPC. White solid (dashed) lines indicate statistically significant increase (decrease) at the 90% level comparing to the climatology.

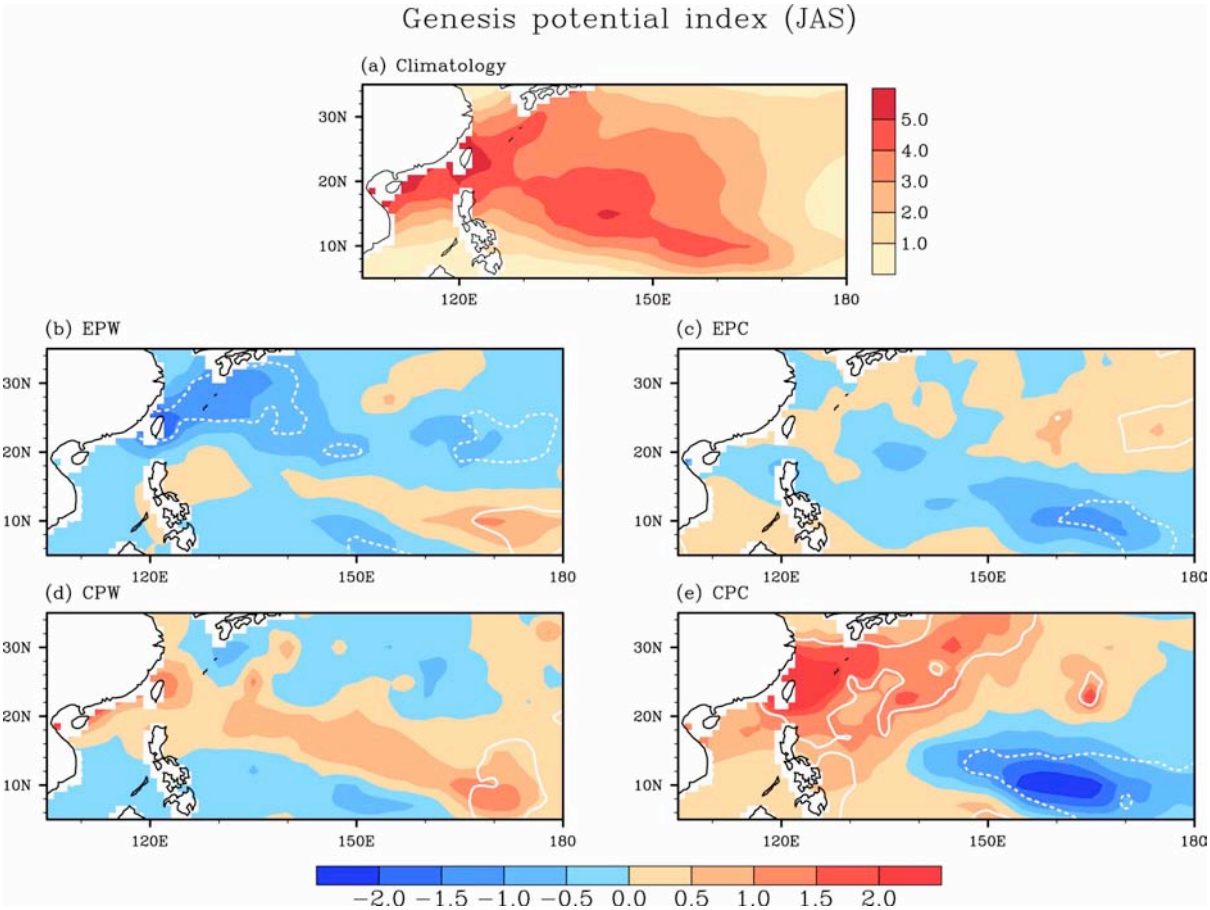

Figure 8. TC genesis potential index (GPI) during the peak season of JAS. Shown are (a) climatological GPI and GPI anomalies in (b) EPW, (c) EPC, (d) CPW, and (e) CPC. White solid (dashed) lines indicate statistically significant increase (decrease) at the 90% level comparing to the climatology.

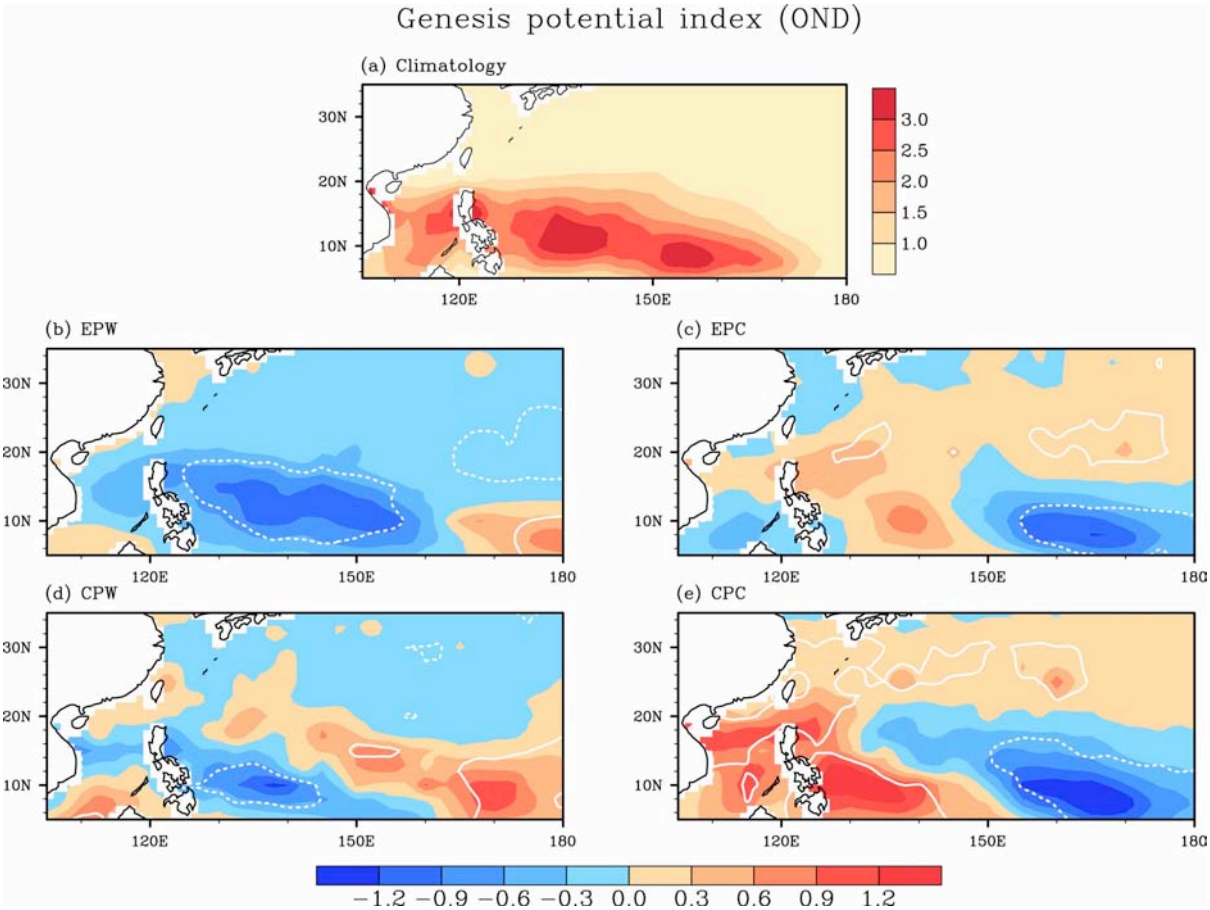

Figure 9. TC genesis potential index (GPI) during the late season of OND. Shown are (a) climatological GPI and GPI anomalies in (b) EPW, (c) EPC, (d) CPW, and (e) CPC. White solid (dashed) lines indicate statistically significant increase (decrease) at the 90% level comparing to the climatology.

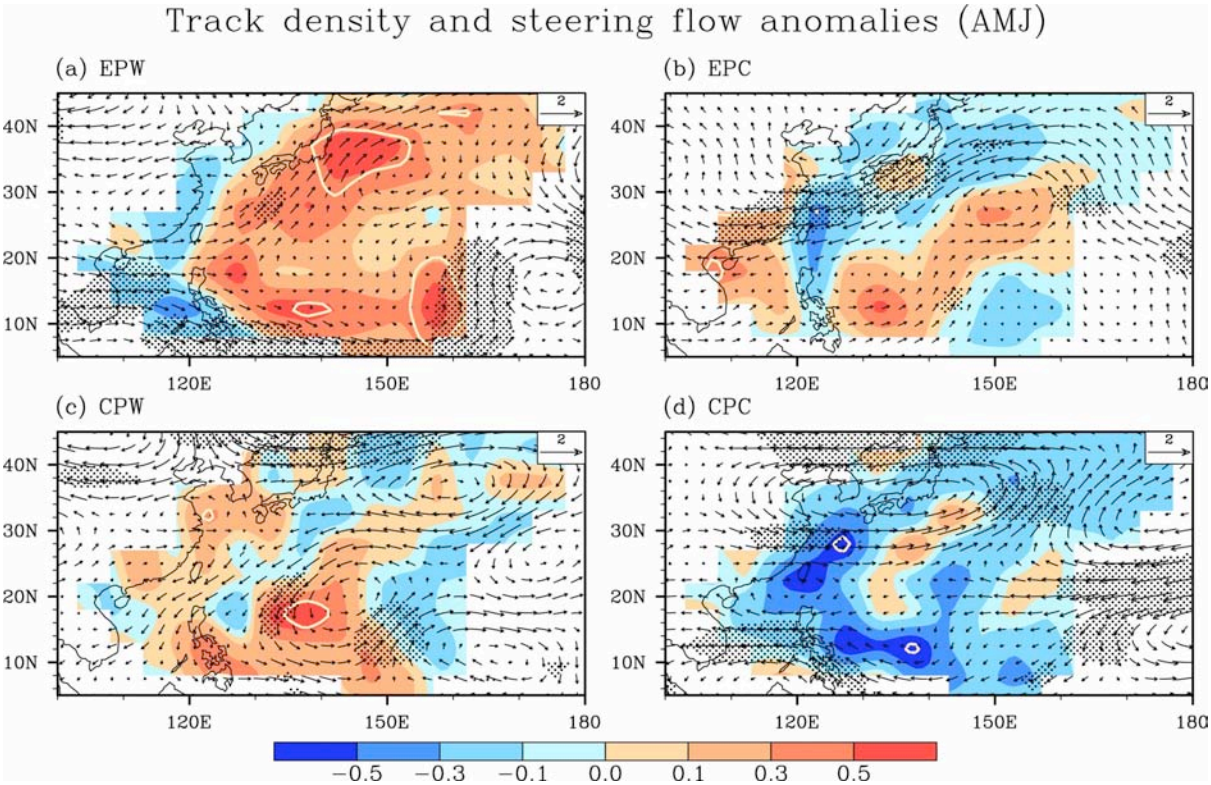

Figure 10. TC track density (the number) and steering flow anomalies (m/s) during the early season of AMJ. Shown are in (a) EPW, (b) EPC, (c) CPW, and (d) CPC. The steering flow is calculated as the vertically-integrated wind from 850 hPa to 300 hPa, normalized by (850-hPa - 300-hPa). White contours and stippling indicate statistically significant at the 90% level for track density and steering flow, respectively.

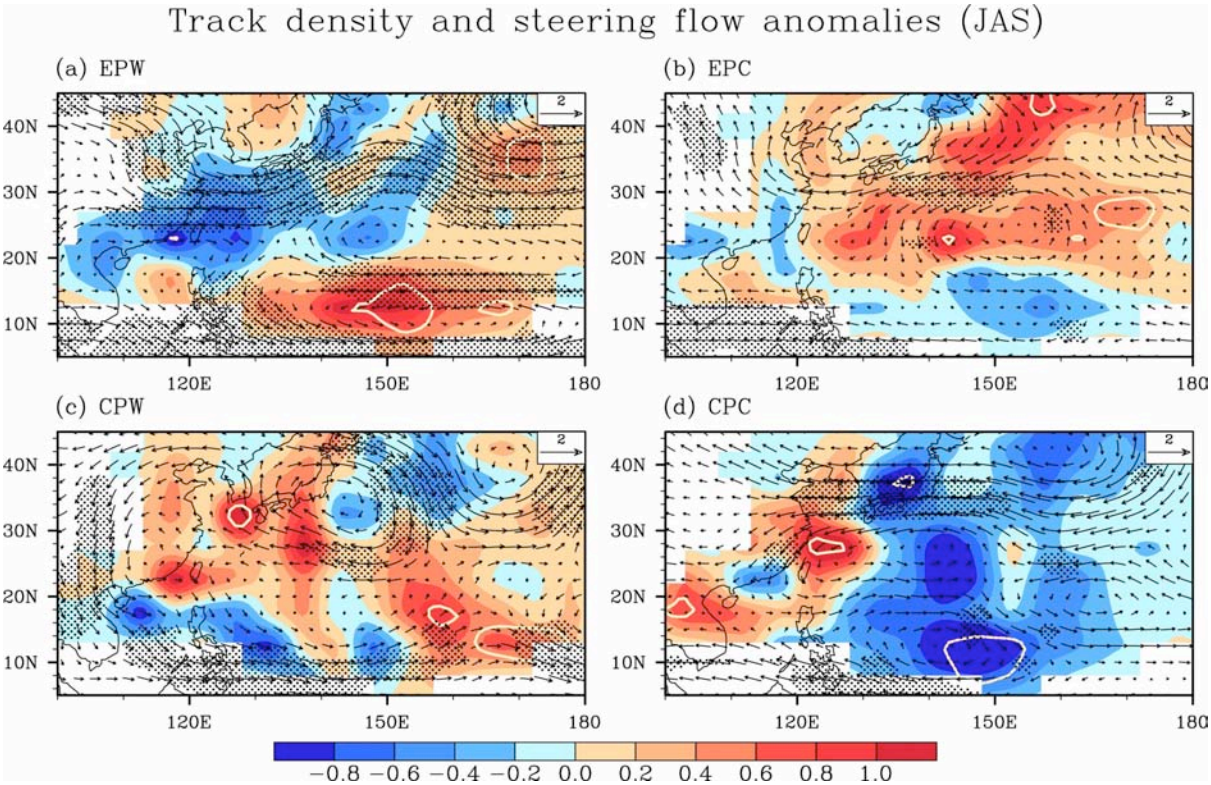

Figure 11. TC track density (the number) and steering flow anomalies (m/s) during the peak season of JAS. Shown are in (a) EPW, (b) EPC, (c) CPW, and (d) CPC. The steering flow is calculated as the vertically-integrated wind from 850 hPa to 300 hPa, normalized by (850-hPa - 300-hPa). White contours and stippling indicate statistically significant at the 90% level for track density and steering flow, respectively.

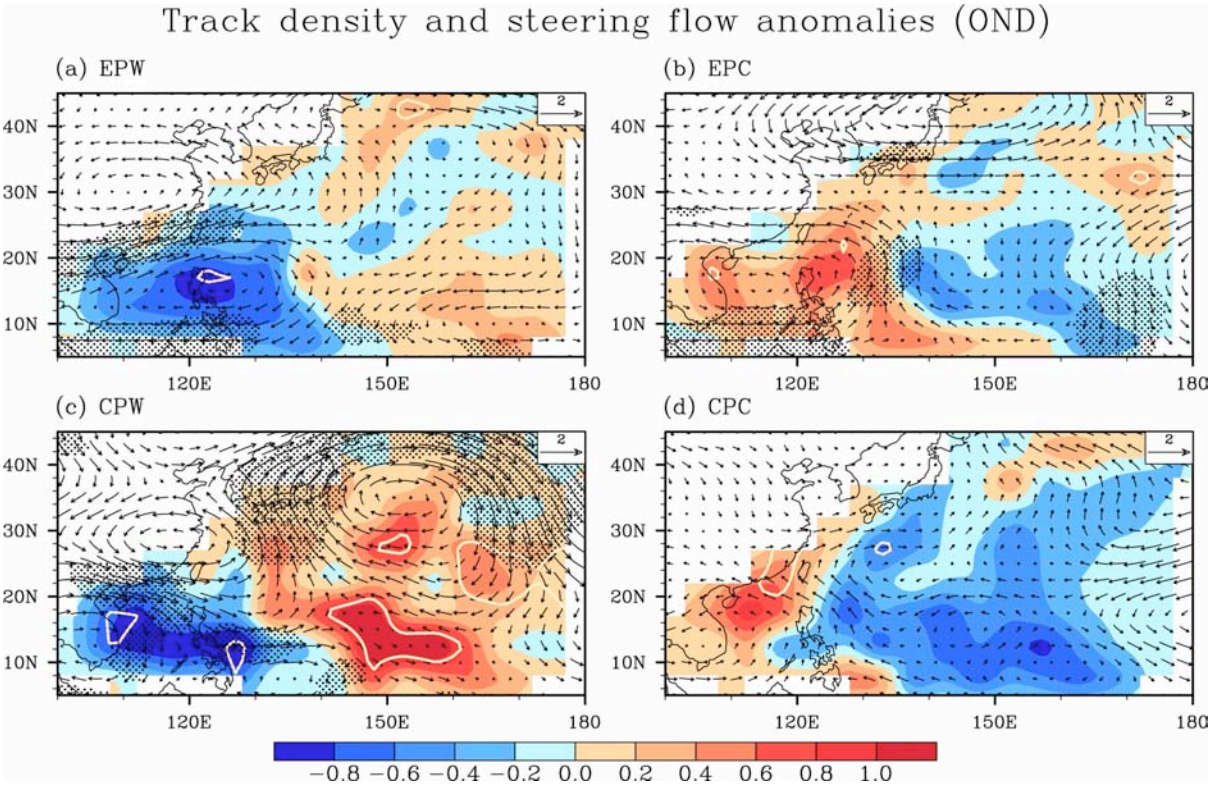

Figure 12. TC track density (the number) and steering flow anomalies (m/s) during the late season of OND. Shown are in (a) EPW, (b) EPC, (c) CPW, and (d) CPC. The steering flow is calculated as the vertically-integrated wind from 850 hPa to 300 hPa, normalized by (850-hPa - 300-hPa). White contours and stippling indicate statistically significant at the 90% level for track density and steering flow, respectively.

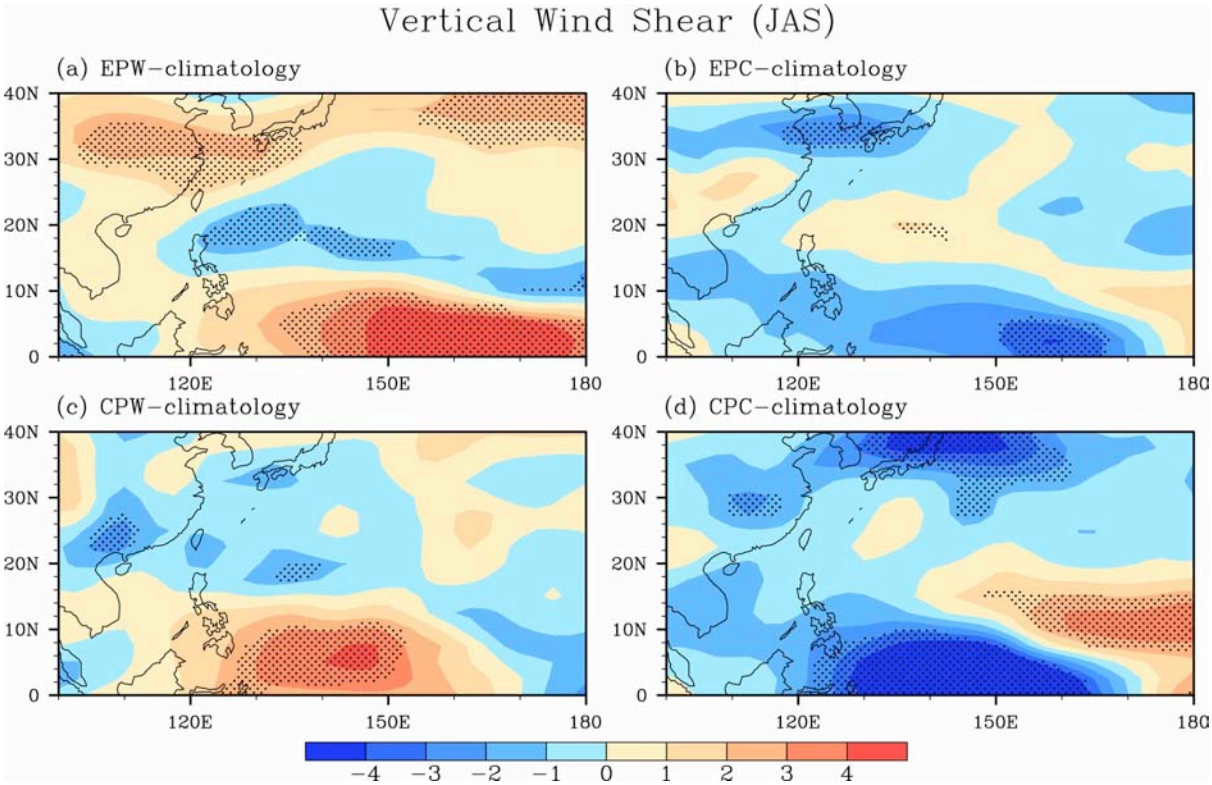

Figure 13. Vertical wind shear (VWS) difference (m/s) between ENSO events and climatology during the peak season of JAS. Shown are in (a) EPW, (b) EPC, (c) CPW, and (d) CPC. The stippling indicates statistically significant at the 90% level. The VWS is calculated as the magnitude of the vector difference between winds at 200 hPa and 850 hPa.